Nuclear Engineering and Technology 48 (2016) 218–227

Available online at ScienceDirect

Nuclear Engineering and Technology

journal homepage: www.elsevier.com/locate/net

Original Article

Modeling of Reinforced Concrete for Reactor Cavity Analysis under Energetic Steam Explosion Condition

Seung Hyun Kim [a], *Yoon-Suk Chang* [a,*], *Yong-Jin Cho* [b], *and Myung Jo Jhung* [b]

[a] *Department of Nuclear Engineering, Kyung Hee University, 1732 Deogyeong-daero, Giheung-gu, Yongin-si, Gyeonggi-do 446-701, Republic of Korea*

[b] *Korea Institute of Nuclear Safety 34 Gwahak-ro, Yuseong-gu, Daejeon 305-338, Republic of Korea*

ARTICLE INFO

Article history:
Received 29 June 2015
Received in revised form
9 September 2015
Accepted 10 September 2015
Available online 2 December 2015

Keywords:
Equivalent Homogeneous Concrete Property
Finite Element Analysis
Reactor Cavity
Structural Failure Criteria
Yield Criterion

ABSTRACT

Background: Steam explosions may occur in nuclear power plants by molten fuel–coolant interactions when the external reactor vessel cooling strategy fails. Since this phenomenon can threaten structural barriers as well as major components, extensive integrity assessment research is necessary to ensure their safety.

Method: In this study, the influence of yield criteria was investigated to predict the failure of a reactor cavity under a typical postulated condition through detailed parametric finite element analyses. Further analyses using a geometrically simplified equivalent model with homogeneous concrete properties were also performed to examine its effectiveness as an alternative to the detailed reinforcement concrete model.

Results: By comparing finite element analysis results such as cracking, crushing, stresses, and displacements, the Willam–Warnke model was derived for practical use, and failure criteria applicable to the reactor cavity under the severe accident condition were discussed.

Conclusion: It was proved that the reactor cavity sustained its intended function as a barrier to avoid release of radioactive materials, irrespective of the different yield criteria that were adopted. In addition, from a conservative viewpoint, it seems possible to employ the simplified equivalent model to determine the damage extent and weakest points during the preliminary evaluation stage.

1. Introduction

Steam explosions may occur in nuclear power plants due to molten fuel–coolant interactions when the external reactor vessel cooling strategy [1,2] fails. This phenomenon can threaten the integrity of the reactor cavity, penetration piping, and support structures as well as major components. Even though extensive research has been performed to predict the effects of steam explosions, it remains a possible hazard due to the complexity of physical phenomena and harsh environmental thermal–hydraulic conditions [3,4].

The steam explosion phenomenon is usually classified into four phases: premixing, triggering, propagation, and expansion processes [5,6]. At first, in the premixing phase, the

* *Corresponding author.*
E-mail address: yschang@khu.ac.kr (Y.-S. Chang).

http://dx.doi.org/10.1016/j.net.2015.09.009
1738-5733/Copyright © 2015, Published by Elsevier Korea LLC on behalf of Korean Nuclear Society.

molten jet breaks up, and a coarsely mixed region of molten corium and coolant is formed. The explosive system can remain in this metastable state until the melt is quenched or a steam explosion is triggered. The triggering event is a disturbance that destabilizes the vapor film around a melt particle, allowing liquid–liquid contact and leading to locally enhanced heat transfer, pressurization, and fine fragmentation. During the propagation phase, an escalation process takes place resulting from heat transfer after the triggering event. Finally, during the expansion phase, thermal energy of the coolant is converted into mechanical energy so that the high-pressured mixture countered by the inertial constraints governs the possibility of a steam explosion. If the localized high pressure is quickly stabilized, only the kinetic energy transmitted to materials around the interaction zone becomes the unique damaging agent [3].

To resolve the remaining open issues on the fuel–coolant interaction) processes and their effects on steam explosion energetics, the IFCI [7] and TEXAS [8] analysis codes were developed. In addition, the OECD project of Steam Explosion REsolution for Nuclear Applications (SERENA), consisting of experimental and analytical parts, was launched in 2007 to enhance the understanding and modeling techniques of the fuel–coolant interaction key features [3,9]. However, despite these previous researches, structural evaluation methods and criteria for steam explosions were not clearly defined for reactor applications. Structural evaluation requires appropriate models either to delineate complicated reinforced concrete material behaviors or to reduce computational cost during the initial design stage.

In this context, the present numerical study focuses on the yield criteria under a typical postulated steam explosion condition. The influence of yield criteria are investigated through parametric finite element (FE) analyses, and subsequent structural assessments are also performed for the reactor cavity in a nuclear power plant with an electric power capacity of 1,400 MWe. Moreover, to examine the effectiveness of an alternative to the detailed reinforcement model, simplified FE analyses with homogeneous concrete properties are carried out and their results, such as cracking, crushing, stresses, and displacements, are compared with each other in detail.

2. Theory of concrete structural evaluation

2.1. Yield criteria of concrete material

Even though various material models have been proposed for concrete structural analyses, four representative yield criteria, Wiliam-Warnke (WW) [10], Mohr-Coulomb (MC) [11], Drucker-Prager (DP) [12], Winfrith (W) [13], were examined in this study. All the governing equations to define yield criteria can be represented by the stress tensor that is closely related to the following stress invariants (I_i; i = 1, 2, and 3) and deviatoric stress invariants (J_i; i = 1, 2, and 3):

$$I_1 = \sigma_{11} + \sigma_{22} + \sigma_{33}$$

$$I_2 = \sigma_{11}\sigma_{22} + \sigma_{22}\sigma_{33} + \sigma_{33}\sigma_{11} - \sigma_{12}^2 - \sigma_{23}^2 - \sigma_{31}^2 \quad (1)$$

$$I_3 = \sigma_{11}\sigma_{22}\sigma_{33} + 2\sigma_{12}\sigma_{23}\sigma_{31} - \sigma_{12}^2\sigma_{33} - \sigma_{23}^2\sigma_{11} - \sigma_{31}^2\sigma_{22}$$

$$J_1 = S_{11} + S_{22} + S_{33}$$

$$J_2 = \frac{1}{3}I_1 - I_2 \quad (2)$$

$$J_3 = \frac{2}{27}I_1^3 - \frac{1}{3}I_1I_2 + I_3$$

Historically, the Willam–Warnke model has been adopted to predict failures of concrete and cohesive–frictional materials such as rock and soil, the yield criterion of which can be defined as a functional form:

$$f(I_1, J_2, J_3) = 0 \quad (3)$$

If the details of the second and third deviatoric stress invariants (J_2 and J_3) as well as the first stress invariant (I_1) are provided, the yield surface of the Willam–Warnke yield criterion can be specified as follows:

$$f = \sqrt{J_2} + \lambda(J_2, J_3)\left(\frac{I_1}{3} - \mathrm{B}\right) = 0 \quad (4)$$

where λ is a function of J_2 and J_3, and B is the hydrostatic stress parameter dependent on material properties and friction angle. This model may be interpretable as a combination of the Mohr–Coulomb and Drucker–Prager yield criteria.

The Mohr–Coulomb yield criterion was developed to deal with the response of concrete in which compressive loads are prevailing. It has been reported that this model leads to a relatively accurate prediction, and its yield surface can be expressed as follows [11]:

$$f(I_1, J_2, \theta) = \frac{1}{3}I_1\sin\phi + \sqrt{J_2}\sin\left(\theta + \frac{\pi}{3}\right) + \frac{\sqrt{J_2}}{\sqrt{3}}\cos\left(\theta + \frac{\pi}{3}\right)\sin\phi - c\cos\phi \quad (5)$$

where ϕ and c are material parameters, and θ is the stress state parameter dependent on the deviatoric stress invariants.

$$\theta = \frac{1}{3}a\cos\left(\frac{3\sqrt{3}}{2}\frac{J_3}{J_2^{3/2}}\right) \quad (6)$$

Eqs. (5) and (6) represent straight lines, as the yield surface of the Mohr–Coulomb yield criterion has an irregular hexagonal shape, which is enveloped by the smooth yield surface of the Drucker–Prager model.

The Drucker–Prager yield criterion [12] describes the response of concrete subjected to compression moderately well and provides a smooth yield surface. This model defines the yield surface as a function of material parameters α and y:

$$\sqrt{J_2} + \alpha I_1 + \mathrm{y} = 0. \quad (7)$$

$$\alpha = \frac{2\sin\phi}{\sqrt{3}(3 - \sin\phi)}, \quad \mathrm{y} = \frac{6\cos\phi}{\sqrt{3}(3 - \sin\phi)}. \quad (8)$$

where ϕ is the friction angle between 30° and 37°, approximately, which can be determined by experimental data. In the present study, the value of the friction angle was set to 37° conservatively.

The Winfrith yield criterion is based on a shear failure theory, and its yield surface can be specified by stress invariant, deviatoric stress invariant, and material properties such as compressive strength (f_c') and tensile strength (f_t'):

$$F(I_1, J_2, \cos 3\theta) = a\frac{J_2}{\left(f_c'\right)^2} + \lambda\frac{\sqrt{J_2}}{f_c'} + b\frac{I_1}{f_c'} - 1. \quad (9)$$

where a and b are constants that control the meridional shape of the yield surface of the Winfrith yield criterion. Since it can be defined as a function of J_2 and $\sqrt{J_2}$, unlike other yield surfaces that are dependent only on $\sqrt{J_2}$, the concrete material behaviors can be solved as a quadratic form [Eq. (10)]:

$$\frac{\sqrt{J_2}}{f_c'} = \frac{-B + \sqrt{B^2 - 4AC}}{f_c'}. \quad (10)$$

where $A = b$, $B = \lambda$, and $C = b(I_1/f_c') - 1$. Thus, once the parameters a, b, and λ are determined, the independent parameter I_1 varies according to compressive and tensile loads. Fig. 1 shows a comparison of yield surfaces defined by the four yield criteria.

2.2. *Structural failure criteria*

It is important to assure the structural integrity of nuclear power plants under various accident conditions to avoid the release of radioactive materials. Particularly, in case of the reactor cavity, the steel liner plate is installed as a barrier and jointed with the reinforced concrete to prevent its penetration by severe loadings and harsh environments. Thus, it is anticipated that compressive and tensile loads that cause local inelastic deformation and damage to the concrete material in the form of cracking and crushing are acceptable as long as the reactor cavity barrier is not breached.

Determination of the reactor cavity failure is not easy because it consists of a liner plate and reinforced concrete that show complex ductile and brittle behaviors. In general, two types of failures can be identified [14]. One is a failure of the rebar and liner plate, which is associated with the exhaustion of material ductility of the steel. The other is a concrete failure associated with penetration. The latter is much more subjective than the former in judging the time reached to failure condition from the structural analysis.

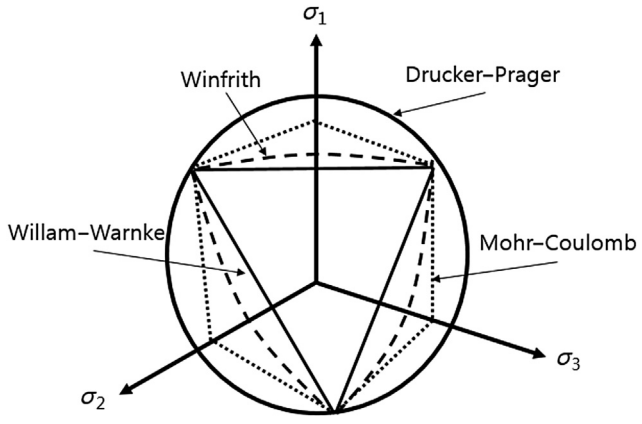

Fig. 1 – Yield surfaces defined by four yield criteria.

In this study, the condition whether the reactor cavity fails or not was determined by structural FE analyses. Especially, for the concrete material, a stress-based failure criterion was derived from the yield criteria. A limiting value of 0.25 was newly proposed for the ratio of concrete failure, defined as the cracked and crushed volumes divided by the initial undamaged whole volume of the concrete. As described before, cracking and crushing of concrete are closely related to ultimate tensile and/or compressive strengths, and their amounts depend on the yield criteria. By contrast, 0.05 was selected as the limiting value of the strain-based failure criterion for the rebar and liner plate made of carbon and austenitic stainless steels, of which the technical basis and rationale were described in NEI 07-13 [14]. If one of these failure criteria for the concrete, rebar, and liner plate is violated, from a conservative point of view, it can be regarded as a loss of structural integrity of the reactor cavity under the steam explosion condition.

3. Numerical analyses

3.1. *Analysis conditions*

Analysis conditions such as failure modes, explosion locations, and corium/coolant characteristics were determined according to a previous study [8]. In particular, among diverse steam explosion scenarios, the most severe case (side vessel failure mode, middle location explosion, corium temperature of 3,500 K, and coolant temperature of 273 K) was selected as the typical one. Fig. 2 shows loading histories, at three representative positions, due to the steam explosion applied to the corresponding inner wall of the reactor cavity as loading conditions. They were obtained from a computational fluid dynamics analysis combined with the Hicks–Menzies

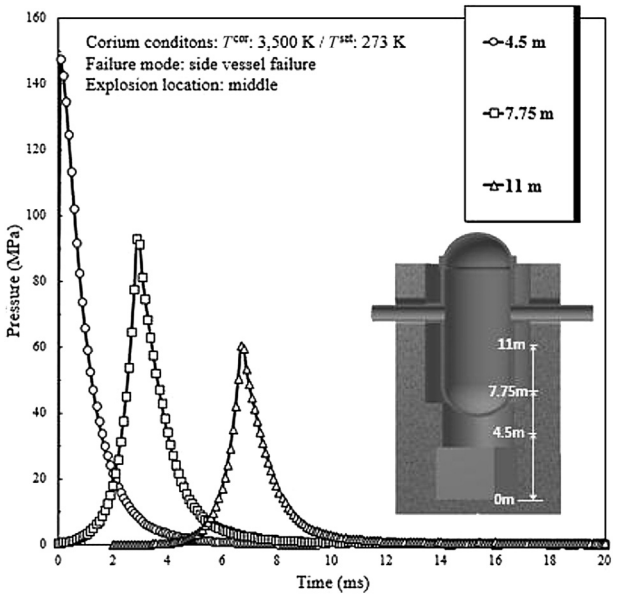

Fig. 2 – Representative loading histories under steam explosion condition.

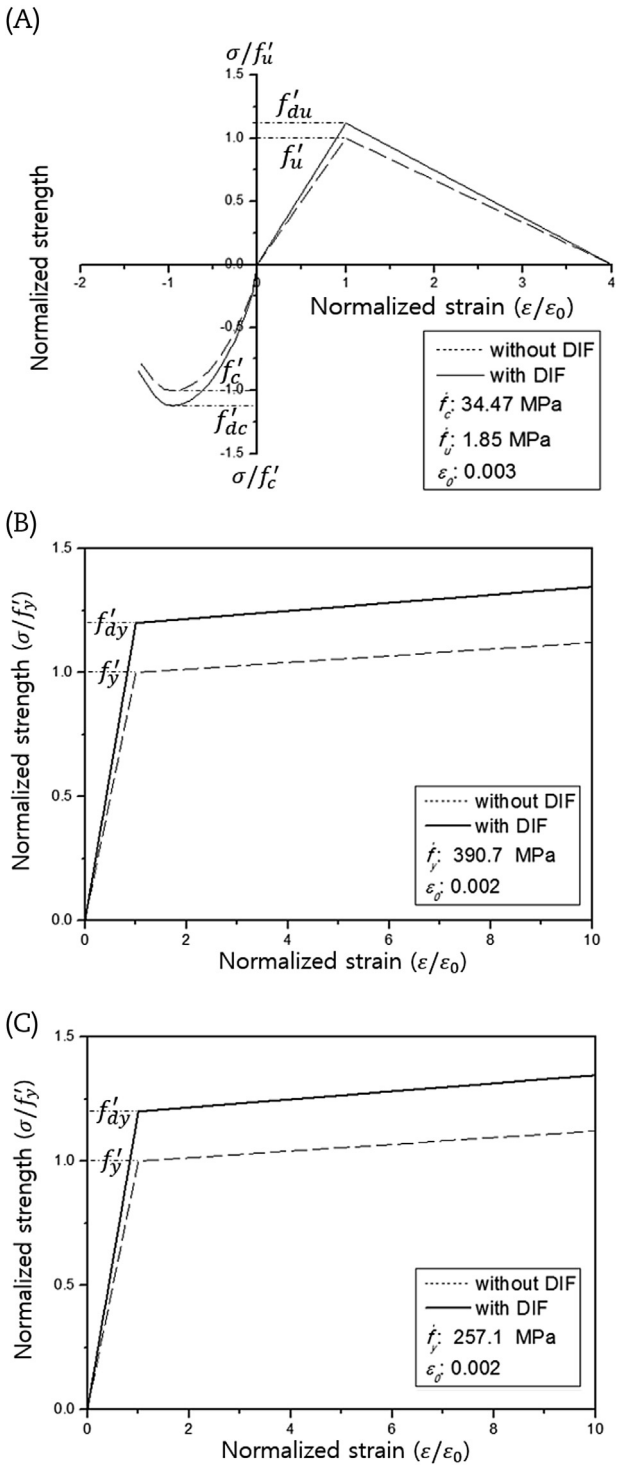

Fig. 3 – Normalized stress–strain relations: (A) concrete, (B) rebars, and (C) liner plates.

thermodynamic approach [3], taking into account the micro-interaction zone concept [4].

A uniaxial compressive strength (f'_c) of 34.47 MPa and a strain (ε_0) at this compressive strength of 0.003 were taken as representative properties for the concrete of the reactor cavity, according to the American Concrete Institute code [15,16]. Since Poisson's ratio (ν_c) of the concrete under uniaxial compressive stress ranges from 0.15 to 0.22, the value of ν_c was assumed to be 0.2 in this study. In addition, due to the difficulty in measuring them, the uniaxial tensile strength (f'_u) and the initial modulus of elasticity (E_c) of concrete were determined using the following general equations as a function of the compressive strength [17]:

$$f'_u = 0.33\sqrt{f'_c}\,\text{MPa} \tag{11}$$

$$E_c = 4,700\sqrt{f'_c}\,\text{MPa} \tag{12}$$

Fig. 3 depicts stress–strain relations of the concrete, rebars, and liner plates. In the figure, tensile stresses were normalized by f'_u, compressive stresses by f'_c, and strains by ε_0. The absolute values incorporating dynamic effects were employed for FE analyses to reflect elastic–plastic material behaviors according to the isotropic hardening rule. Meanwhile, material properties equivalent to the homogenous concrete could be obtained using Eq. (13) [17]. They were used for comparative analyses of the actual reactor cavity with the reinforced concrete.

$$S_c^{eq} = (1 - V_s)S_c + V_s S_s. \tag{13}$$

where S_c^{eq} is the equivalent strength of homogeneous concrete, and V_s is the volume fraction of rebar, determined to be 0.081. S_c and S_s are the strengths of concrete and rebar, respectively. Material properties of the rebar, liner plate, and associated components and supports were the same as those reported in a previous research [3]. In details, the kinematic hardening model with bilinear elastic–plastic behavior was adopted because of the rapid strain change caused by explosive loading.

To incorporate the dynamic effects, the moduli of elasticity and strengths of the reactor cavity as well as penetration piping and support structures were determined by considering the dynamic increase factor (DIF; 1.00–1.29) in Eq. (14) [3,16]:

$$f'_{dy} = f'_y(\text{DIF}_y), \quad f'_{du} = f'_u(\text{DIF}_u) \tag{14}$$

where f'_y and f'_u are, respectively, the yield strength and ultimate tensile strength under the static loading condition, and f'_{dy} and f'_{du} are the corresponding ones under the dynamic loading condition, like a steam explosion. Fig. 3 represents the normalized stress–strain relations by taking into account the DIFs of concrete, rebars, and liner plates, representatively. Table 1 summarizes the material properties used in the structural analyses taking into account the DIF values.

3.2. *Modeling and analysis method*

Systematic structural analyses of the reactor cavity were performed by using the FE model, the dimensions of which were approximately 19 m × 11 m × 20 m [18]. Fig. 4 shows FE models of the reactor cavity used in the analyses; rebars embedded in the concrete were modeled using 22,914 beam elements with 23,314 nodes. The cavity wall was modeled by employing 408,858 eight-node three-dimensional concrete elements consisting of 438,994 nodes, and the liner plates

Table 1 – Material properties used in structural assessment.

Material		Modulus of elasticity (GPa)	Poisson's ratio	Yield strength (MPa)	Ultimate tensile strength (MPa)
Concrete		31.12	0.2	38.68[a]	2.18
Rebar	A615 Gr.60	199.95	0.3	468.84	620.52
Steel liner plate	SA516 Gr.60	199.95	0.3	303.36	455.05
Homogeneous concrete		44.79	0.2	73.52[a]	57.93

[a] Compressive strength.

were modeled by employing 39,830 shell elements consisting of 43,102 nodes. A contact condition was assigned between the inner surfaces of the cavity wall and the linear plate by sharing nodes. As a boundary condition, the bottom side of the reactor cavity was fully fixed.

In order to reduce the burden of complex modeling of the whole reactor cavity, a geometrically simplified FE mesh was also developed by eliminating the rebar assembly and assigning the aforementioned equivalent homogeneous concrete properties. This model, applicable to the determination of the damage extent and weakest points during the preliminary evaluation stage, was employed for comparative analyses to examine its effectiveness as an alternative to the actual reinforced concrete structure. Therefore, in the present

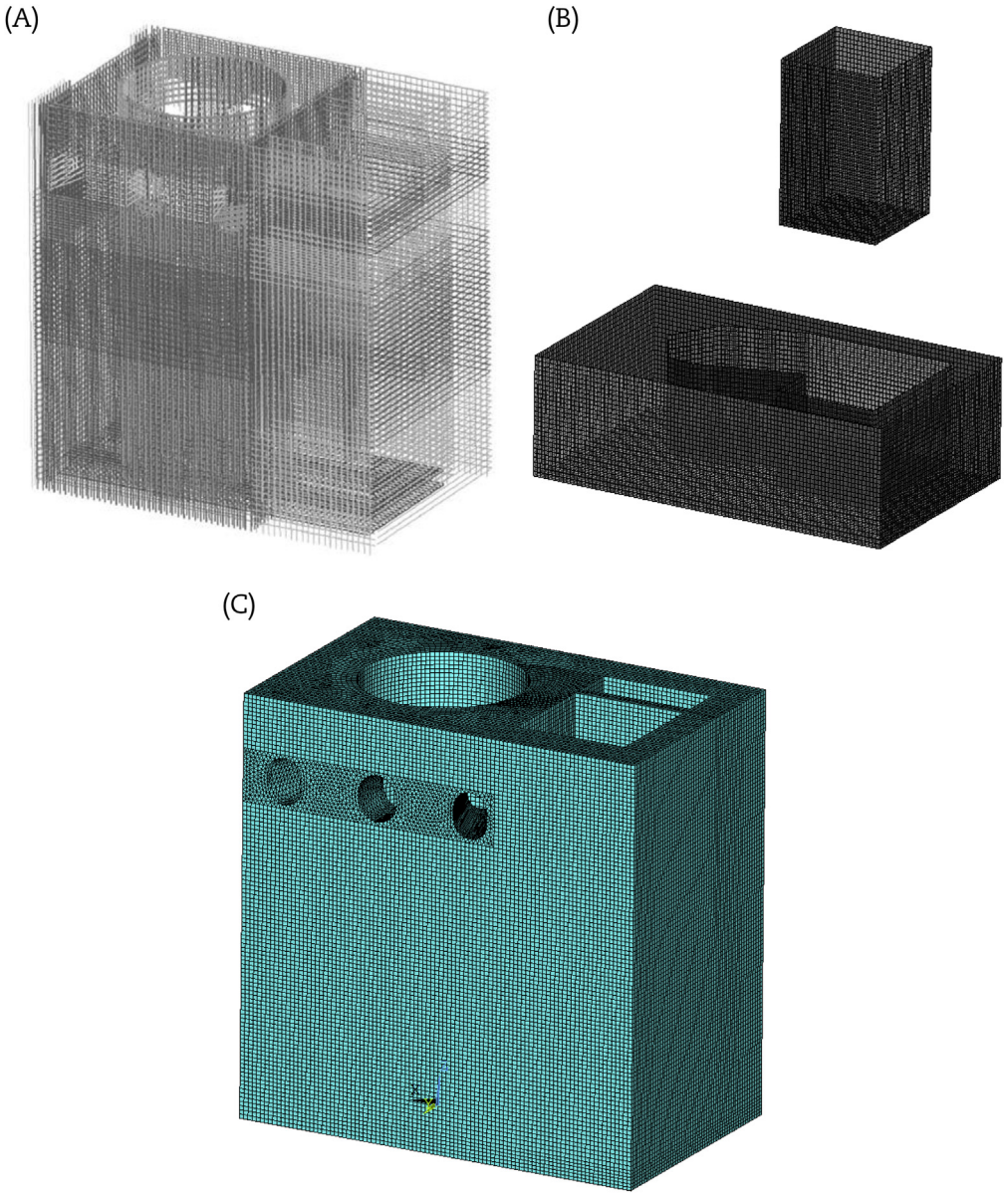

Fig. 4 – FE models of reactor cavity. (A) Rebars. (B) Liner plates. (C) Concrete.

Table 2 – Structural analysis results by using detailed reinforced models.

	Willam–Warnke concrete model	Mohr–Coulomb concrete model	Drucker–Prager concrete model	Winfrith concrete model
Max. von Mises stress (MPa) (concrete)	21.12	15.54	12.52	18.12
Max. equivalent strain (concrete)	0.0050	0.0035	0.0032	0.0048
Ratio of concrete failure	0.11	0.07	0.05	0.10
Max. von Mises stress (MPa) (rebar)	602.84	592.25	593.18	596.25
Max. equivalent strain (rebar)	0.031	0.028	0.028	0.029
Max. von Mises stress (MPa) (steel liner plate)	404.95	405.95	406.10	405.50
Max. equivalent strain (steel liner plate)	0.011	0.011	0.011	0.011

study, a total of eight structural FE analyses were carried out by combining the four yield criteria with the reinforced or homogeneous concrete properties.

4. Results and discussion

4.1. *Analysis results of detailed reinforced models*

Table 2 compares structural analysis results, such as the maximum von Mises stress and equivalent strain of each component, and the ratio of concrete failure using the detailed reinforced models. As summarized in the table, the Willam–Warnke and Drucker–Prager models provided the highest and lowest values for all concrete-related parameters, respectively. Their differences were about 41% for the stress, 36% for the strain, and 55% for the ratio of concrete failure. In all the analysis cases, the maximum von Mises stresses were less than the compressive strength of concrete and the equivalent strains were minimal.

Figs. 5 and 6 depict the cracking and crushing regions obtained from the detailed reinforced models in red at the section of explosion position (at a height of 4.5 m from the bottom, as shown in Fig. 2). In spite of the cracking and crushing that occurred due to high-pressure waves, the reinforced concrete was not penetrated, and the ratios of concrete failure were less than 0.25 regardless of the yield criteria. Under the typical steam explosion condition, the minimum ligaments through the cavity wall thickness were roughly 35% in the Willam–Warnke model and 60% in the Drucker–Prager model. In addition, the maximum displacement at the weakest point of concrete nearest to the explosion location was also large when the Willam–Warnke model was employed and its maximum value was approximately 80 mm. As shown in Fig. 7, fluctuating displacements were rapidly attenuated and stabilized at 20 milliseconds after the steam explosion.

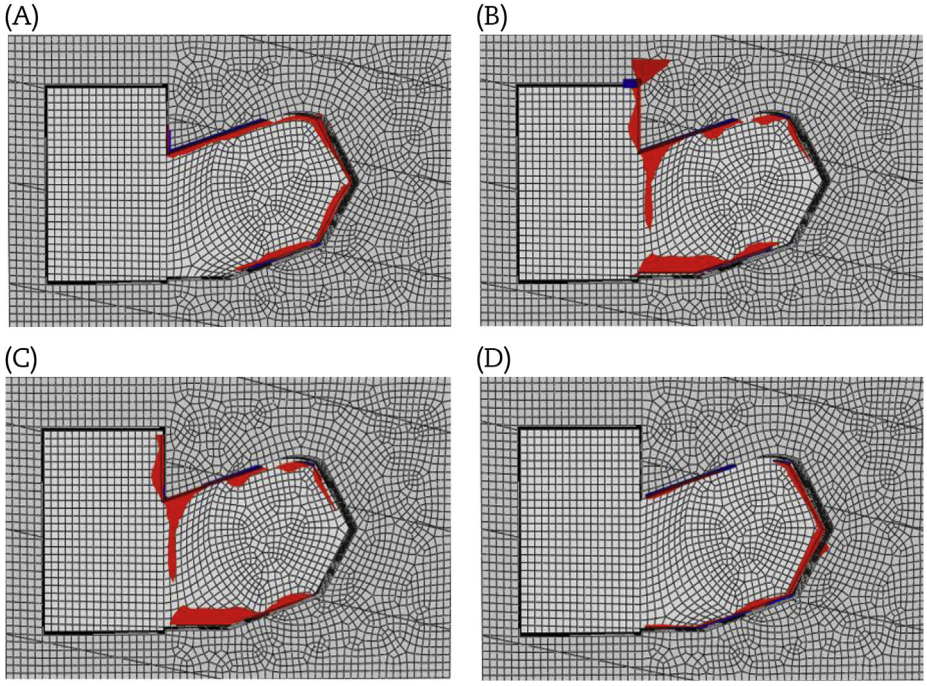

Fig. 5 – Cracking regions obtained from detailed reinforced models. (A) Willam–Warnke concrete model. (B) Mohr–Coulomb concrete model. (C) Drucker–Prager concrete model. (D) Winfrith concrete model.

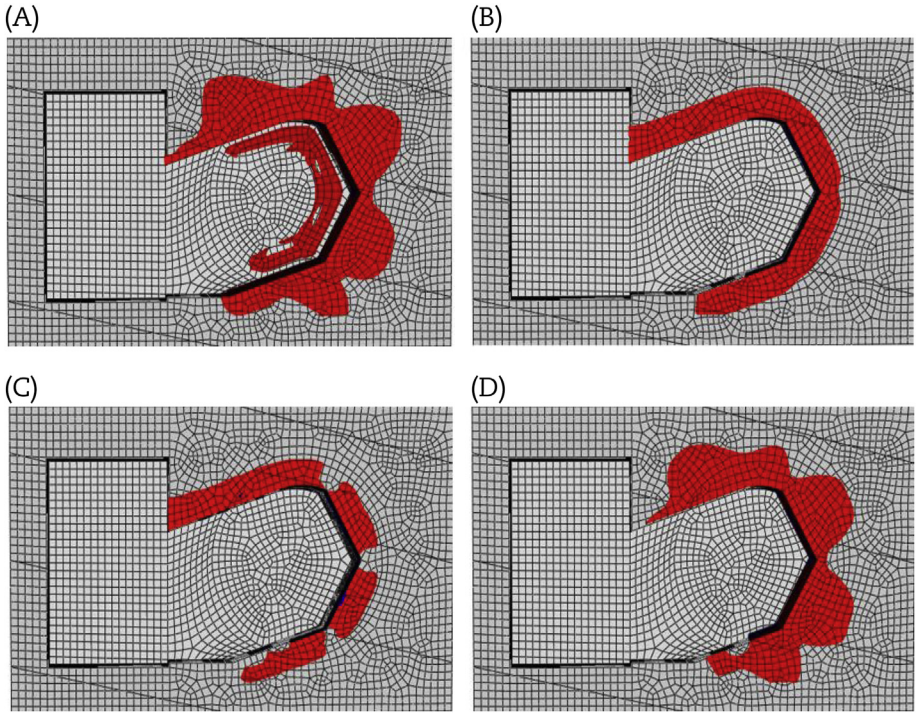

Fig. 6 – Crushing regions obtained from detailed reinforced models. (A) Willam–Warnke concrete model. (B) Mohr–Coulomb concrete model. (C) Drucker–Prager concrete model. (D) Winfrith concrete model.

With regard to the rebar and liner plate, although there were some differences in the maximum stresses and strains, the influence of the yield criteria was not as significant as anticipated. Their differences were less than 2% for the stress and 10% for the strain with regard to the rebar, and both were less than 0.3% with regard to the liner plate. In all the analysis cases, von Mises stresses exceeded their yield strengths but were less than ultimate tensile strengths. The resulting equivalent strains were less than the corresponding limiting value of failure criterion of 0.05, which was explained in the second section.

4.2. *Analysis results of simplified reinforced models*

Table 3 compares the structural analysis results using the simplified equivalent models, in which the same trend as that of the detailed reinforced models were observed. The Willam–Warnke and Drucker–Prager yield criteria provided the highest and lowest values for all concrete related parameters, respectively. Their differences were about 22% for the stress, 23% for the strain, and 46% for the ratio of concrete failure. Overall, the analysis results by the simplified equivalent models were somewhat more conservative than those by the

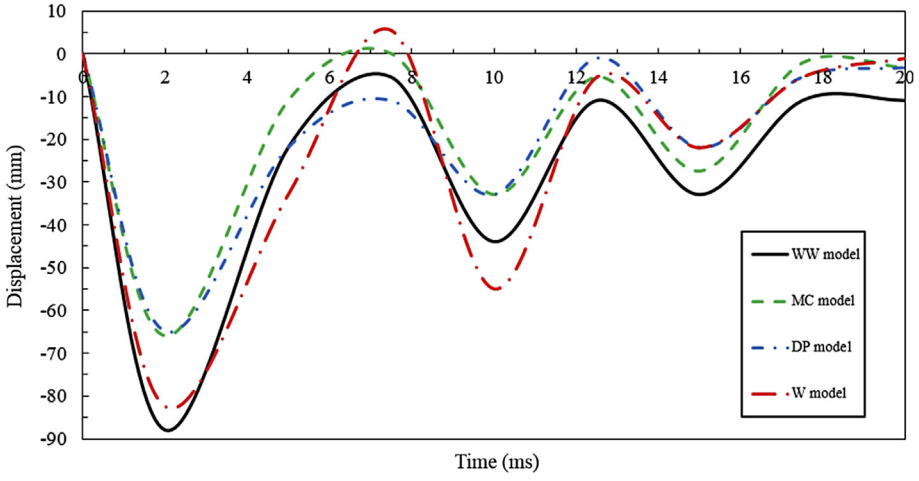

Fig. 7 – Resulting displacements obtained from detailed reinforced models.

Table 3 – Structural analysis results using simplified equivalent models.

	Willam–Warnke concrete model	Mohr–Coulomb concrete model	Drucker–Prager concrete model	Winfrith concrete model
Max. von Mises stress (MPa) (concrete)	80.18	63.56	62.52	77.98
Max. equivalent strain (concrete)	0.0080	0.0063	0.0062	0.0078
Ratio of concrete failure	0.13	0.09	0.07	0.11
Max. von stress (MPa) (steel liner plate)	403.85	404.8	405.2	405.4
Max. equivalent strain (steel liner plate)	0.011	0.011	0.011	0.011

detailed reinforced models. Particularly, the maximum von Mises stress values exceeded the compressive strength of concrete, while the equivalent strains were still not so much.

Figs. 8 and 9 depict the cracking and crushing regions obtained from the simplified equivalent models at the same location as that of the detailed reinforced models. Similar to other analysis parameters, the cracking and crushing regions increased, but the reinforced concrete was not penetrated, and the ratios of concrete failure were less than 0.25 regardless of the yield criteria. The minimum ligaments through the cavity wall thickness were roughly 30% in the Willam–Warnke model and 57% in the Drucker–Prager model under the typical steam explosion condition. In addition, the maximum displacement at the weakest point of concrete nearest to the explosion location was also large when the Willam–Warnke model was employed, and its maximum value was approximately 90 mm, as shown in Fig. 10.

With regard to the liner plate, like the detailed analysis cases, the influence of the yield criteria was not significant. Their differences were less than 2% for the stress and almost the same for the strain. In all the analysis cases, von Mises stresses exceeded their yield strengths but were less than ultimate tensile strengths. The resulting equivalent strains were less than the corresponding limiting value of failure criterion of 0.05.

4.3. *Discussion*

In actual and hypothetic concrete modeling, it was proved that all the maximum values of concrete-related parameters could be obtained by employing the Willam–Warnke model. These trends of FE analysis results were consistent with the schematic of yield surfaces defined by each yield criterion. It is also available to use the geometrically simplified FE mesh with equivalent homogeneous concrete properties for estimating damage extent and the weakest points during the preliminary evaluation stage because the alternative analyses led to conservative results in all the concrete-related parameters. Subsequently, an opposite trend was observed with regard to the rebar and liner plate. Their stresses and strains were slightly high when the Drucker–Prager yield criterion was employed, which was thought to be due to the effect of interaction with the actual or hypothetic concrete.

On the other hand, two failure criteria were satisfied for the reactor cavity under the steam explosion condition: the limiting failure ratio of the concrete and the limiting strain of the rebar and steel liner plate. The equivalent homogeneous as well as reinforced concrete was not penetrated when cracking and crushing occurred, and all the failure ratios were less than 0.25. In addition, the maximum equivalent strain of the rebar and steel liner plate were also less than the current

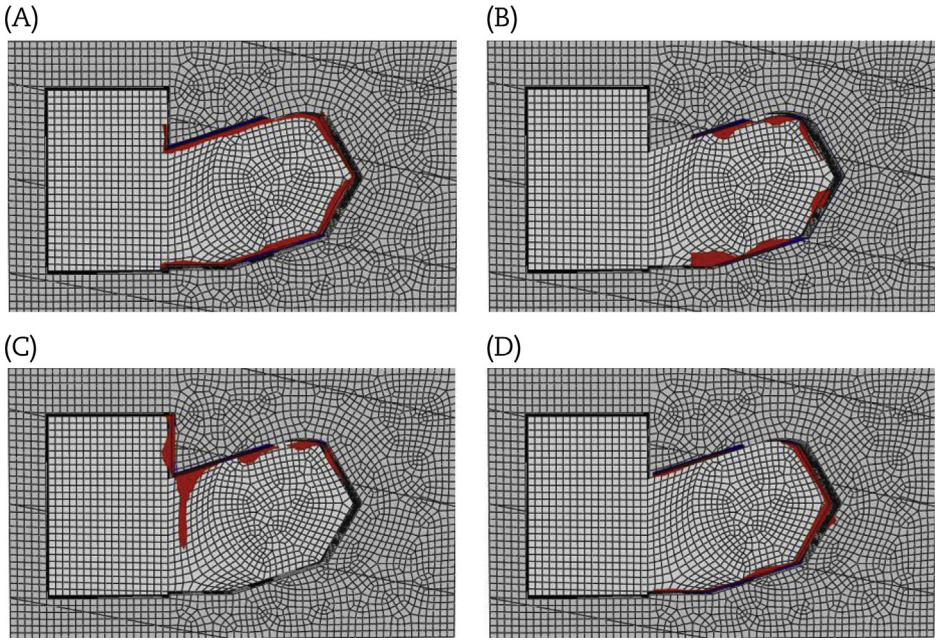

Fig. 8 – Cracking regions obtained from simplified equivalent models. (A) Willam–Warnke concrete model. (B) Mohr–Coulomb concrete model. (C) Drucker–Prager concrete model. (D) Winfrith concrete model.

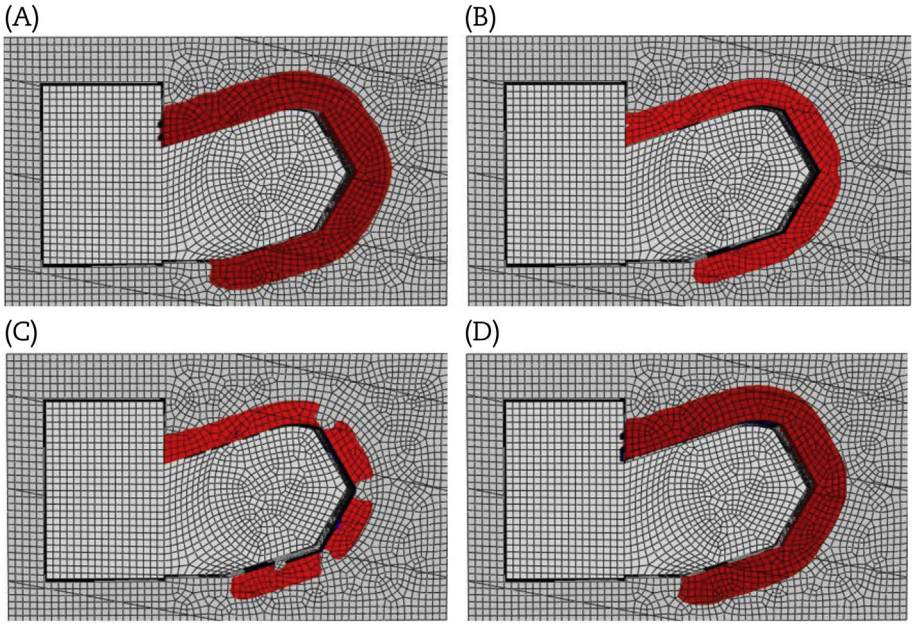

Fig. 9 – Crushing regions obtained from simplified equivalent models. (A) Willam–Warnke concrete model. (B) Mohr–Coulomb concrete model. (C) Drucker–Prager concrete model. (D) Winfrith concrete model.

failure criterion specified in NEI 07-13. However, since the limiting concrete failure ratio of 0.25 and the minimum ligament may be debatable, further investigations to set obvious criteria for the reinforced concrete are anticipated from associated experts in succession to the present study.

5. Conclusion

In this study, the Willam–Warnke, Mohr–Coulomb, Drucker–Prager, and Winfrith yield criteria were investigated for reinforced concrete structures. In addition, relevant failure criteria were examined and applied to a reactor cavity consisting of concrete, rebar, and liner plate under a typical steam explosion condition, from which the following conclusions were derived.

The Willam–Warnke model is recommended for practical use considering uncertainties in severe accident conditions because it provided the highest values of the ratio of concrete failure as well as stresses, strains, and displacements for the concrete. In addition, the effects of yield criteria on the rebar and liner plate were not significant, whereas slightly higher stresses and strains were obtained by the Drucker–Prager model due to interaction with the actual or hypothetic concrete.

Two types of failure criteria for the reactor cavity were satisfied in all analysis cases. Particularly, systematic FE

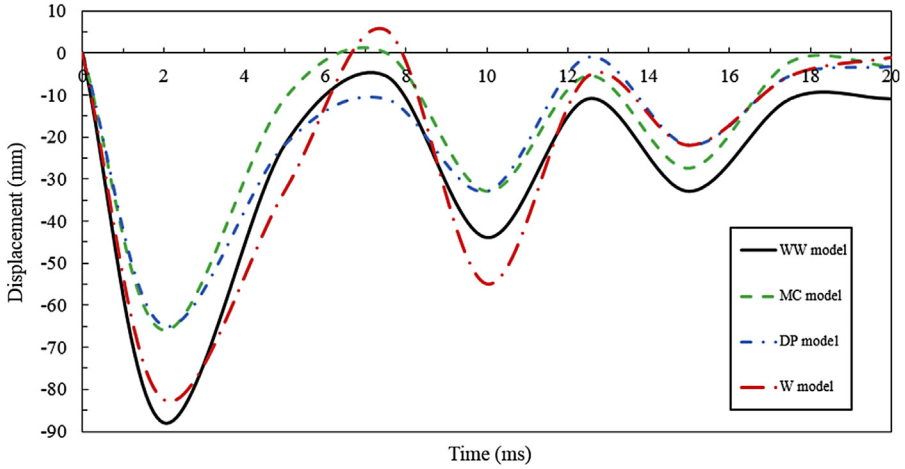

Fig. 10 – Resulting displacements obtained from simplified equivalent models.

analysis results were less than not only the newly proposed ratio of concrete failure limiting value of 0.25, but also the maximum equivalent strain of the rebar and steel liner plate, which is the limiting value of 0.05 as specified in NEI 07-13.

The reactor cavity was not penetrated by the cracking and crushing. However, further investigation on the undamaged ligament was carried out to check the possibility of local failure. The minimum ligaments through the cavity wall thickness were 35% by the Willam–Warnke model and 60% by the Drucker–Prager model in the detailed evaluation, and 30% by the Willam–Warnke model and 57% by the Drucker–Prager model in the simplified evaluation under the typical steam explosion condition.

The reactor cavity sustained its safety function to avoid release of radioactive materials under the typical steam explosion condition, regardless of the yield criteria. Therefore, it seemed possible to use restrictively the simplified FE mesh with equivalent homogeneous concrete properties, for estimating damage extent and the weakest points during the preliminary evaluation stage, from a conservative viewpoint.

Conflicts of interest

The authors declare no conflicts of interest.

Acknowledgments

This work was supported by the Nuclear Safety Research Program through the Korea Radiation Safety Foundation (KORSAFe) and the Nuclear Safety and Security Commission (NSSC), Republic of Korea (Grant No. 1305001).

REFERENCES

[1] J.H. Jung, S.M. An, K.S. Ha, H.Y. Kim, Evaluation of heat-flux distribution at the inner and outer reactor vessel walls under the in-vessel retention through external reactor vessel, Nucl. Eng. Technol. 47 (2015) 66–73.

[2] T.H. Kim, S.H. Kim, Y.S. Chang, Structural assessment of reactor pressure vessel under multi-layered corium formation conditions, Nucl. Eng. Technol. 47 (2015) 351–361.

[3] S.H. Kim, Y.S. Chang, S.C. Song, Y.J. Cho, Structural assessment of fully flooded reactor cavity and penetration piping under steam explosion conditions, Int. J. Press. Vessels Pip. 131 (2015) 36–44.

[4] L. Cizelj, B. Koncar, M. Leskovar, Vulnerability of a partially flooded PWR reactor cavity to a steam explosion, Nucl. Eng. Des. 236 (2006) 1617–1627.

[5] I.G. Cullis, J. Schofield, A. Whitby, Assessment of blast loading effects—types of explosion and loading effects, Int. J. Press. Vessels Pip. 87 (2010) 493–503.

[6] L. Cizelj, B. Koncar, M. Leskovar, Estimation of ex-vessel steam explosion pressure load, Nucl. Eng. Des. 239 (2009) 2444–2458.

[7] Sandia National Lab, IFCI 7.0 models and correlations, SAND99-1000, 1999.

[8] M.L. Corradini, C.C. Chu, I. Huhtiniemi, J. Murphy, S. Nilsuwankosit, J. Tang, S. Wang, User's Manual for TEXAS-V One Dimensional Transient Fluid Model, University of Wisconsin-Madison, 2002.

[9] OECD/NEA, OECD research programme on fuel–coolant interaction, SERENA Final Report, 2007.

[10] K.J. Willam, E.P. Warnke, Constitutive models for the triaxial behavior of concrete, Proc. Int. Assoc. Bridge Struct. Eng. 19 (1975) 1–30.

[11] A.J. Abbo, A.V. Lyamin, S.W. Sloan, J.P. Hambleton, A C2 continuous approximation to the Mohr–Coulomb yield surface, Int. J. Sol. Struct. 48 (2010) 3001–3010.

[12] J.L. Cela, Analysis of reinforced concrete structures subjected to dynamic loads with a viscoplastic Drucker–Prager model, Appl. Math. Model 22 (1998) 495–515.

[13] N.S. Ottosen, A failure criterion for concrete, J. Eng. Mech. 103 (1977) 527–535.

[14] Nuclear Energy Institute, Methodology for performing aircraft impact assessments for new plant designs, NEI 07-13, 2011.

[15] ACI Committee 349, Code Requirements for Nuclear Safety Related Concrete Structures, American Concrete Institute, Washington, USA, 2010.

[16] ACI Committee 318, Building Code Requirements for Structural Concrete, American Concrete Institute, Washington, USA, 2002.

[17] H.T. Hu, Y.H. Lin, Ultimate analysis of PWR prestressed concrete containment subjected to internal pressure, Int. J. Press. Vessels Pip. 83 (2006) 161–167.

[18] ANSYS Civil FEM, Introduction of Civil FEM, Ver. 13.0, ANSYS Inc., 2012.